A Statistical Analysis Of Temperature Mechanisms And Patterns For Coral Bleaching

Undergraduate Project Report

by,

Manas Kumar

Roll Number - 220611
Mathematics & Scientific Computing, IIT Kanpur

Under the supervision of

Dr. Arnab Hazra

Assistant Professor, IIT Kanpur

DEPARTMENT OF MATHEMATICS AND STATISTICS
INDIAN INSTITUTE OF TECHNOLOGY KANPUR

DECLARATION

I hereby declare that the work presented in the project report entitled **A Statistical Analysis Of Temperature Mechanisms And Patterns For Coral Bleaching** is written by me in my own words and contains my own or borrowed ideas. At places, where ideas and words are borrowed from other sources, proper references and acknowledgements, as applicable, have been provided. To the best of my knowledge this work does not emanate from or resemble work created by person(s) other than those mentioned and acknowledged herein.

Name and Signature: Manas Kumar (220611)
Date: 11th April 2025

Arnab Hazra

Arnab Hazra (Supervisor)

Acknowledgement

I would like to express my sincere gratitude to my project supervisor, **Dr. Arnab Hazra**, Department of Mathematics and Statistics, IIT Kanpur, for his invaluable guidance, constant encouragement, and insightful feedback throughout the course of this project.

His deep knowledge and clear vision greatly enriched my understanding of the subject and provided a strong foundation for this undergraduate project. I am grateful for the opportunity to work under his mentorship, which has been both intellectually stimulating and personally rewarding.

I would also like to thank the Department of Mathematics and Statistics, IIT Kanpur, for providing the necessary resources and an excellent research environment that made this work possible.

Manas Kumar
Roll Number: 220611
B.S. Mathematics and Scientific Computing
Indian Institute of Technology Kanpur

Contents

1 Literature Review

The use of machine learning (ML) in spatial environmental modeling has witnessed remarkable growth over the past decade, driven by the increasing availability of high-resolution spatial datasets and the need for accurate predictions in complex ecological systems. Among the diverse ML algorithms, Random Forests (RF) have gained substantial popularity due to their robustness, ability to handle high-dimensional data, and capacity to model nonlinear relationships and interactions among variables **Hengl et al.** 2018; **Cutler et al.** 2007. However, a critical limitation of standard RF models lies in their foundational assumption that observations are independent and identically distributed (i.i.d.), an assumption that seldom holds in spatial datasets where observations are often correlated due to underlying spatial processes **Li et al.** 2011. When spatial autocorrelation is ignored, it can result in biased estimates and misleading assessments of model performance. This has motivated the development of a suite of spatial adaptations of RF to appropriately account for the spatial structure in the data. Some of the more commonly used strategies involve the inclusion of spatial coordinates or derived spatial covariates into the feature set, while others rely on post-hoc residual kriging techniques, such as RF residual kriging (RF-RK) and RFsp, to incorporate spatial dependence into the prediction surface **Hengl et al.** 2018. However, these approaches often lack a rigorous theoretical underpinning, treating spatial dependence as an auxiliary feature rather than an intrinsic component of the modeling framework. In a significant advancement, **Saha et al.** 2023 introduced the Random Forest-Generalized Least Squares (RF-GLS) methodology, which directly integrates spatial dependence into the RF learning algorithm through a generalized least squares (GLS) formulation. This approach not only addresses the theoretical limitations of previous spatial extensions but also improves predictive performance by explicitly modeling the spatial correlation structure, especially under conditions characterized by Matérn Gaussian processes. The RF-GLS framework demonstrates consistency and efficiency in parameter estimation, providing a robust tool for spatial prediction in environmental sciences. Parallel to improvements in modeling techniques, evaluation methodologies have also evolved to better account for spatial dependence during model validation. Traditional cross-validation techniques, which randomly partition the dataset, tend to overestimate model performance in the presence of spatial autocorrelation. This realization has led to the development of spatially-aware validation approaches, such as spatial blocking **Roberts et al.** 2017; **Valavi et al.** 2019, where data is partitioned into spatial blocks to prevent information leakage between training and testing sets. From a statistical modeling perspective, hierarchical Bayesian models and spatial mixed-effects frameworks offer powerful tools to explicitly represent spatial structure and associated uncertainties **Banerjee et al.** 2014. Generalized additive models (GAMs) have also been employed for their flexibility in capturing smooth, nonlinear covariate effects in spatially varying settings **Wood** 2017. In addition, variable selection remains a core challenge in spatial ML. **Meyer et al.** 2019 emphasized the necessity of choosing covariates that meaningfully reflect underlying spatial processes rather than merely fitting surface-level patterns, a sentiment echoed in earlier studies on spatial interpolation **Li et al.** 2011. Within the specific application domain of coral bleaching, recent research has underscored the importance of accounting for both spatial and temporal dynamics to better understand and predict bleaching events. **Hughes et al.** 2018 documented large-scale changes in coral reef assemblages driven by ocean warming, while **Hoegh-Guldberg et al.** 2017 provided a comprehensive review of how climate change and ocean acidification threaten reef ecosystems. **McClanahan et al.** 2019 examined the complexity of thermal exposure during the 2016 El Niño, showing that traditional metrics like Degree Heating Weeks (DHW) may fall short of capturing the full range of bleaching risks. They argued for more nuanced predictors that consider event duration, intensity patterns, and geographic context. Similarly, **Ainsworth et al.** 2016 demonstrated that prior thermal exposure and site-specific characteristics significantly modulate coral responses to stress events, pointing to the importance of modeling local adaptation and historical resilience. Collectively, these developments affirm that accurately modeling coral bleaching demands more than just high-quality temperature data—it requires integrating spatial dependence both in model structure and validation strategies. The combination of spatially-explicit ML models like RF-GLS with robust, spatially-aware evaluation techniques represents a promising step toward enhancing predictive accuracy, ecological realism, and conservation outcomes in coral reef systems.

2 Understanding the Aim & the Dataset

2.1 Aim

Coral bleaching is a stress response that occurs when extreme thermal conditions lead corals to expel their symbiotic algae (*zooxanthellae*), often resulting in increased susceptibility to mortality. Studies demonstrates that coral bleaching is governed by a complex interplay of multiple environmental stressors rather than being solely a function of cumulative heat exposure. Specifically, variables such as peak high-temperature spells, prolonged periods of cooler temperatures, and the bimodality of temperature distributions were found to be key drivers of bleaching severity. The results underscore that bleaching responses are not strictly determined by static thermal thresholds, but are significantly influenced by the temporal structure of temperature extremes—namely, their frequency, duration, and deviation from localized climatological baselines. This highlights the necessity for more nuanced and context-aware predictive models that can capture the dynamic nature of thermal stress events and better inform conservation strategies.
The primary objective of this project is to investigate the factors influencing coral reef resilience in response to climate change and anthropogenic stressors. The study evaluates the effectiveness of different conservation strategies in mitigating the impacts of environmental changes on coral ecosystems. Specifically, it analyzes the patterns and drivers of coral bleaching events across multiple reef systems, assesses the role of local management interventions in enhancing reef recovery and resilience, investigates the interactions between climate-induced stress and human activities on coral reef health, and provides empirical data to support policy recommendations for sustainable coral reef conservation. By addressing these objectives, the study contributes to a deeper understanding of coral reef dynamics and informs future conservation efforts aimed at preserving marine biodiversity.

The dataset focus on coral bleaching patterns during the 2016 El Niño event across the Indo-Pacific region. This comprehensive dataset represents one of the most extensive coordinated efforts to document coral bleaching responses and the underlying environmental factors that influence bleaching severity.

2.2 Dataset Overview

The dataset contains information from 226 reef sites spanning 60° of latitude and 140° of longitude across the Indo-Pacific region, from East Africa to Fiji. Data was collected through standardized underwater surveys of 30 coral colonies during the peak of the 2016 El Niño/Southern Oscillation thermal anomaly. The surveys were conducted within 21 days of peak thermal anomalies to ensure timely assessment of bleaching impacts.

2.3 Key Variables in the Dataset

The dataset includes 28 environmental variables, categorized as follows:

2.4 Data Collection Methodology

Researchers used standardized underwater survey methods to assess coral bleaching. For each site, they characterized sea surface temperatures (SSTs) in the 90 days before the survey, quantifying the number, duration, and magnitude of anomalous temperatures based on the 10th SST quantile ("cold spells") and 90th SST quantile ("hot spells").

3 Introduction

3.1 Spatially Dependent Data

Spatially dependent data refers to observations that are correlated based on their spatial proximity. This means that the value of a variable at one location is influenced by the values of the same variable at nearby locations. This type of data is common in fields like geography, ecology, and environmental science.

Table 1: Summary of Variables Across Categories

Category	Variable	Description
Location	Location Site X and Y Coordinates Management Habitat Reef Type	Geographic region (e.g., Kolombangara, Kenya fringing) Specific site name within the location Latitude and longitude coordinates Conservation status (e.g., open, restricted, no-take) Reef classification (e.g., lagoon, flat, bank, channel, crest)
Bleaching	Bleach Intensity	Primary response variable measuring coral bleaching severity
Temperature	AvgDHW-90Days MaxDHW-90Days DipStatistic BimodalityCoefficient BimodalityRatio	Average Degree Heating Weeks over 90 days Maximum Degree Heating Weeks over 90 days A measure of temperature distribution Indicates whether temperature distribution is bimodal Ratio of two identified bimodality peaks
Temp. Events	NumHighEvents-90Days HighSpellDuration-90Days MaxHighSpellDuration-90Days AvgHighSpellTemp-90Days HighSpell-Variance LowSpell-Duration-90Days DHD-90Days	Number of high-temperature events exceeding the 90th percentile Average duration of high-temperature events Maximum duration of high-temperature events Average temperature during high-temperature events Variance of high-temperature events Average duration of low-temperature events Degree heating days
Community	CCA	A multivariate index of coral community composition

Spatially dependent data can be modeled using the spatial linear mixed model:

$$Y = X\beta + w(\ell) + \varepsilon$$

where Y is the response variable, X is a matrix of covariates, β is a vector of fixed effects coefficients, $w(\ell)$ is a spatial random effect at location ℓ, and ε is the error term.

For the spatial random effect $w(\ell)$, a Gaussian Process with a Matérn covariance function is often used:

$$\text{Cov}(w(\ell_i), w(\ell_j)) = \sigma^2 \frac{2^{1-\nu}}{\Gamma(\nu)} \left(\frac{\sqrt{2\nu} d}{\rho} \right)^{\nu} K_\nu \left(\frac{\sqrt{2\nu} d}{\rho} \right)$$

where $d = ||\ell_i - \ell_j||$ is the distance between locations ℓ_i and ℓ_j, ν is the smoothness parameter, σ^2 is the variance, ρ is the range parameter, $\Gamma(\nu)$ is the gamma function, and K_ν is the modified Bessel function of the second kind.

3.2 Bootstrapping Methods

Bootstrapping is a resampling technique used to estimate the distribution of a statistic by resampling with replacement from the observed data. This method is widely used in statistical inference and machine learning to improve model robustness.

3.2.1 Standard Bootstrapping

Given a dataset $D = \{X_1, X_2, ..., X_n\}$ of size n, standard bootstrapping involves the following steps:

1. Draw n samples with replacement from D to create a bootstrap sample $D^* = \{X_1^*, X_2^*, ..., X_n^*\}$.

2. Compute the statistic of interest (e.g., mean, variance, regression coefficient) on D^*.

3. Repeat the above steps B times to obtain B bootstrap estimates.

4. Compute the empirical distribution of the bootstrap estimates to approximate the true distribution.

3.2.2 GLS Bootstrapping Approach

The Generalized Least Squares (GLS) bootstrapping method accounts for spatial dependence in the data. Unlike standard bootstrapping, GLS bootstrapping incorporates the covariance structure estimated from the data to create more realistic resampling distributions.

Mathematical Formulation: Given the spatial regression model:

$$Y = X\beta + \varepsilon, \quad \text{where} \quad \varepsilon \sim \mathcal{N}(0, \Sigma)$$

where Σ is the covariance matrix capturing spatial dependence.

The GLS estimator is given by:

$$\hat{\beta}_{GLS} = (X^T \Sigma^{-1} X)^{-1} X^T \Sigma^{-1} Y$$

The GLS bootstrapping procedure consists of:

1. Estimate the covariance structure $\hat{\Sigma}$ from the residuals of an initial model fit.
2. Transform the response variable:

$$\hat{\Sigma}^{-1/2} Y = (\hat{\Sigma}^{-1/2} X)\beta + \hat{\Sigma}^{-1/2}\varepsilon, \quad \hat{\Sigma}^{-1/2}\varepsilon \sim \mathcal{N}(0, I)$$

$$Y^* = X^* \hat{\beta} + Z, \quad Z \sim \mathcal{N}(0, I)$$

3. Resample Z to generate multiple bootstrap samples.
4. Refit the model on each bootstrap sample and compute $\hat{\beta}_{GLS}$.
5. Aggregate bootstrap estimates to compute confidence intervals.

3.2.3 Diagrammatic Representation

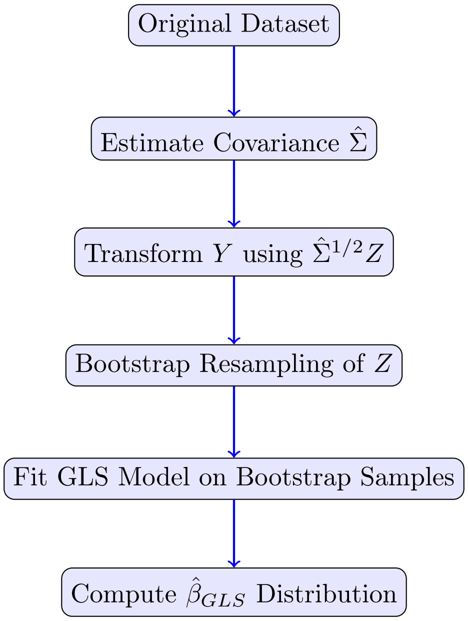
Original Dataset
Estimate Covariance $\hat{\Sigma}$
Transform Y using $\hat{\Sigma}^{1/2} Z$
Bootstrap Resampling of Z
Fit GLS Model on Bootstrap Samples
Compute $\hat{\beta}_{GLS}$ Distribution

4 Preliminary Analysis of Data

4.1 Introduction

According to the data, our target variable is **bleach intensity**

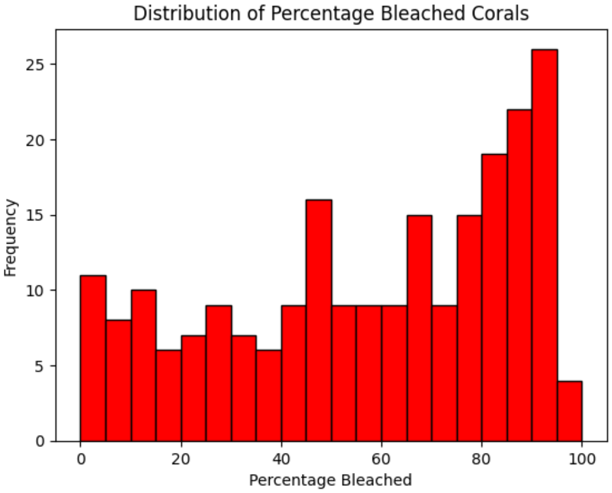

Figure 1: *Percentage of bleached coral vs frequency of locations*

These are the locations at which experiments for coral bleaching intensity were done

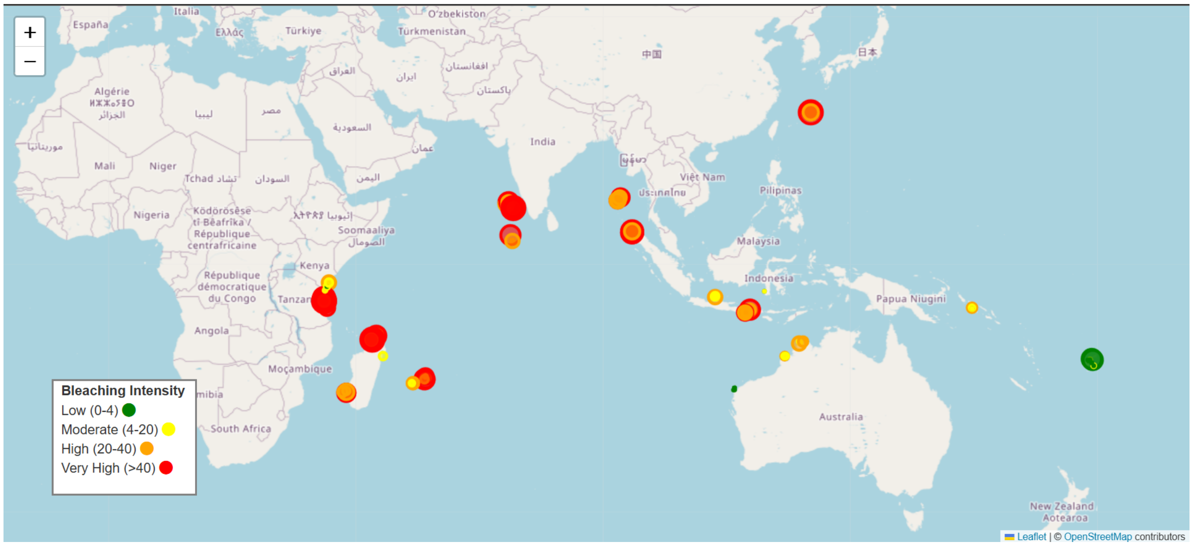

Figure 2:

4.2 Making ML Models to Predict Bleaching Intensity and Analyze Variable Influence

4.2.1 Variables (Covariates) Used in ML Model

`location, site, bleach_intensity, X, Y, management, habitat, average_dhw_90days, max_dhw_90days, dip_Statistic_sst, bimodality_coefficient, bimodality_ratio, n_h_spell_events_90Days, avg_high_spells,` max_high_spell_duration_90days, avg_high_spell_rise_90days, avg_spell_peak, sd_spell_peak, avg_low_spell_duration_90days, dhd_mmmplus1, CA1

4.2.2 Using Simple Linear Regression

- **R^2 Score**: 0.5212
- **Observed vs Predicted Bleach Intensity on Test Data**

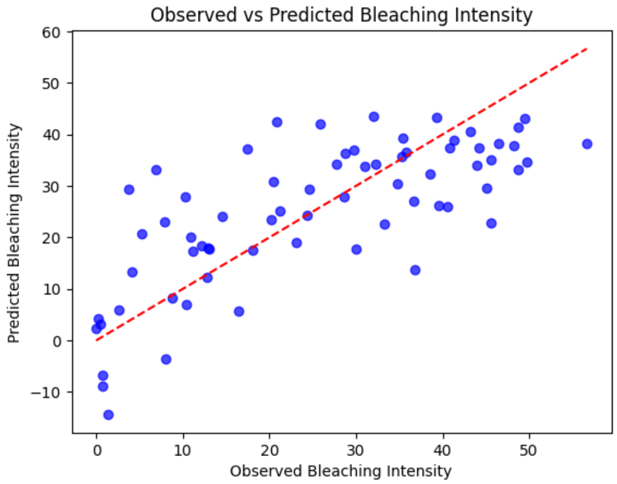

Figure 3: Comparison of observed and predicted bleaching intensity values using simple linear regression model.

- **Relative Influence of Variables**

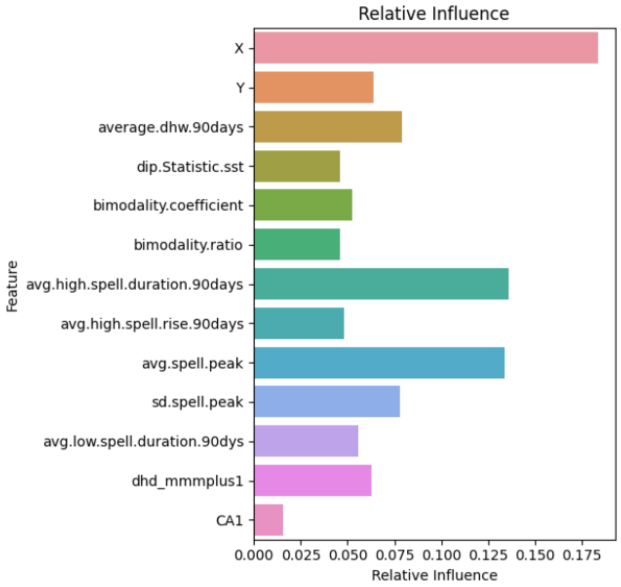

Figure 4: Variable importance ranking from the linear regression model showing relative contribution to bleaching intensity prediction.

- **Issues with the Current Model**:

  - The model fails to account for **spatial dependence**, where neighboring locations might share similar bleaching intensities due to common environmental factors.
  - The R^2 score of **0.52** indicates that nearly half of the variance in bleaching intensity remains unexplained, suggesting missing variables or nonlinear relationships.
  - The model assumes **independent observations**, which may not be valid in a spatial dataset where data points are geographically connected.

4.2.3 Using Spatial Linear Regression through PySAL library

- **R^2 Score** : 0.6740
- **Limitations of the model :**
  - The model struggles to capture **non-linear relationships** and complex spatial dependencies, which may lead to inaccurate predictions for non-stationary spatial processes.
  - The R^2 value of **0.6740** indicates that the model does not fully explain the variability in the data, suggesting the presence of unaccounted factors or missing predictors.
  - Residual dispersion and potential **heteroscedasticity** suggest that the model may not handle varying spatial relationships effectively.

4.2.4 Using Generalized Additive Model (GAM) through PyGAM Library

- **R^2 Score**: 0.8423
- **Observed vs Predicted Bleach Intensity on Test Data**

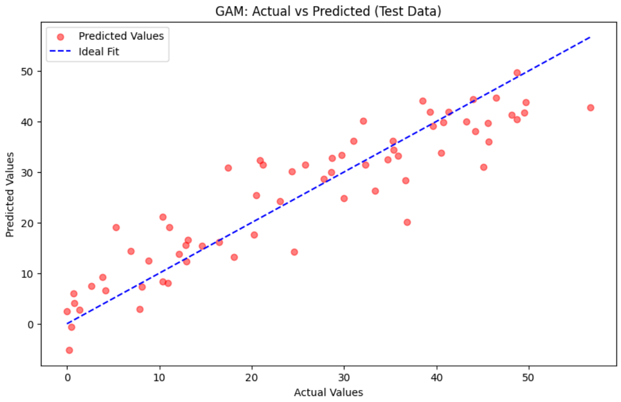

Figure 5: Comparison of observed and predicted bleaching intensity values using GAM model, showing improved fit over linear regression.

- **Advantages of GAM**:
  - Accommodates **nonlinear relationships** between predictors and response, offering greater flexibility than linear regression.
  - Achieves a high R^2 score (0.84), demonstrating that the model captures a significant portion of variation in bleaching intensity.
  - Can model **complex interactions** without requiring a predetermined functional form.
- **Issues with the Current Model**:
  - Still does not account for **spatial dependence**, potentially overlooking geographic correlations in bleaching intensity.

- Despite its flexibility, GAM does not inherently capture **spatial heterogeneity**, which might limit its predictive power for location-based patterns.

4.2.5 Using Clustering Methods to Incorporate Spatial Dependency (K-Means/DBSCAN)

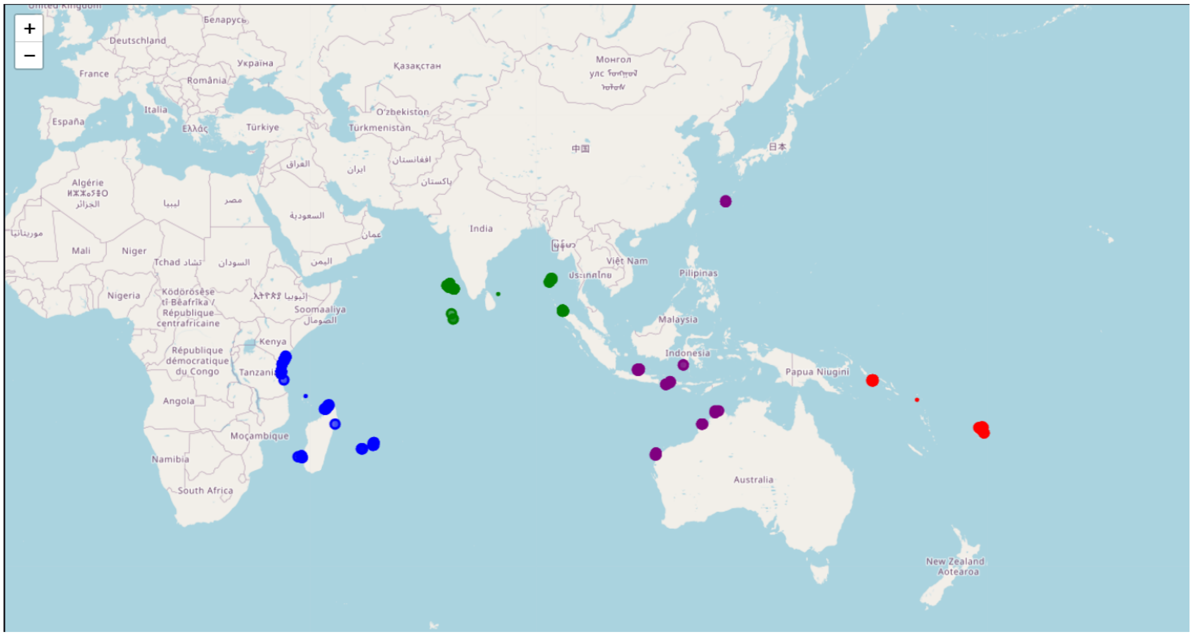

Figure 6: Spatial clustering of sampling locations showing distinct regional patterns in the dataset.

- **Using Random Forest for These Clusters**
  - R^2 for cluster 1: 0.6847
  - R^2 for cluster 2: 0.4875
  - R^2 for cluster 3: 0.5676
  - R^2 for cluster 4: 0.7420
  - Weighted R^2: 0.5804

- **Why Random Forest Instead of Simple Linear Regression?**
  - Random Forest captures **non-linear relationships** and complex interactions, while Simple Linear Regression assumes **linearity**.
  - It effectively handles **missing data** and provides **feature importance**, which is crucial in spatial models.
  - Unlike Linear Regression, which assumes **homoscedasticity**, Random Forest is robust to **heteroscedasticity**.
  - Clustering (K-Means/DBSCAN) helps to account for **spatial dependence**, making Random Forest more suitable for prediction.

- **Limitations of Clustering-Based Random Forest Method**
  - **Arbitrary Cluster Boundaries**: Clustering algorithms impose strict spatial boundaries, grouping data into discrete clusters. This approach ignores spatial relationships between adjacent clusters, leading to discontinuities.

- **Loss of Within-Cluster Variability**: Once clusters are formed, all observations within a cluster are treated similarly. This reduces the ability to model fine-grained spatial effects within each cluster.
- **Ignoring Random Spatial Effects**: Clustering does not explicitly model random variations in spatial data.
- **Cluster Size Sensitivity**: The number of clusters significantly impacts model performance. Too few clusters ignore spatial heterogeneity, while too many may cause overfitting.

4.2.6 Future Direction

To overcome these limitations, we will combine **Random Forest** with a **Random Effects model** to capture both inter-cluster and intra-cluster spatial variability. This approach requires a thorough understanding of Random Forest methodology and implementation of mixed-effects modeling techniques to account for spatial autocorrelation at multiple scales.

5 Random Forest Methodology

5.1 Theoretical Foundation of Random Forests

Random forests represent an ensemble learning method that combines multiple decision trees to produce more accurate and stable predictions. Random forests address overfitting issues common in individual decision trees while maintaining their interpretability advantages. The algorithm employs two key randomization techniques: (1) **bootstrap aggregating (bagging)** of the training data for each tree, and (2) **random selection of features at each split.**

5.1.1 Mathematical Formulation

Let $\mathcal{D} = \{(\mathbf{x}_i, y_i)\}_{i=1}^n$ represent a training dataset with n observations, where $\mathbf{x}_i \in \mathbb{R}^p$ is a p-dimensional feature vector and y_i is the response variable. A random forest constructs an ensemble of T decision trees, denoted as $\{h_1(\mathbf{x}), h_2(\mathbf{x}), \dots, h_T(\mathbf{x})\}$.

For regression problems, the random forest prediction for a new observation $\mathbf{x}$ is given by:

$$\hat{f}_{RF}(\mathbf{x}) = \frac{1}{T}\sum_{t=1}^{T} h_t(\mathbf{x}) \tag{1}$$

For classification problems with K classes, the prediction is made by majority voting:

$$\hat{f}_{RF}(\mathbf{x}) = \text{mode}\{h_1(\mathbf{x}), h_2(\mathbf{x}), \dots, h_T(\mathbf{x})\} \tag{2}$$

Each tree $h_t(\mathbf{x})$ is constructed from a bootstrap sample $\mathcal{D}_t^*$ of the original dataset $\mathcal{D}$. During tree construction, at each node, a random subset of m features is considered for splitting, where typically $m \approx \sqrt{p}$ for classification and $m \approx p/3$ for regression tasks.

Algorithm 1 Random Forest Algorithm

```
Input: Training data $\mathcal{D} = \{(\mathbf{x}_i, y_i)\}_{i=1}^n$, number of trees $T$, number of features to consider at each split $m$, minimum node size $n_{\min}$
Output: Random forest ensemble $\{h_1, h_2, \ldots, h_T\}$ and prediction function $f(\mathbf{x})$
procedure RandomForest($\mathcal{D}, T, m, n_{\min}$)
    for $t = 1$ to $T$ do
        Generate bootstrap sample $\mathcal{D}_t^* = \{(\mathbf{x}_i^*, y_i^*)\}_{i=1}^n$ from $\mathcal{D}$
        Initialize empty tree $h_t$
        Call GrowTree($h_t, \mathcal{D}_t^*, m, n_{\min}$)
    end for
    return $\{h_1, h_2, \ldots, h_T\}$ and
        $$f(\mathbf{x}) = \frac{1}{T}\sum_{t=1}^{T} h_t(\mathbf{x})$$
    for regression or
        $$f(\mathbf{x}) = \arg\max_y \sum_{t=1}^{T} \mathbf{1}(h_t(\mathbf{x}) = y)$$
    for classification.
end procedure
```

5.2 Bootstrapping in Random Forests

5.2.1 Standard Bootstrapping Approach

The standard bootstrapping procedure in random forests involves drawing n samples with replacement from the original dataset to create each tree's training set. This process generates diverse datasets where some observations appear multiple times while others are excluded.

For a dataset with n observations, the probability that a particular observation is not selected in a bootstrap sample is:

$$P(\text{observation not selected}) = \left(1 - \frac{1}{n}\right)^n \approx e^{-1} \approx 0.368 \tag{3}$$

This means that each bootstrap sample contains approximately 63.2% of the unique observations from the original dataset. The remaining 36.8% of observations not selected for a particular tree are referred to as out-of-bag (OOB) samples and provide a built-in validation set for estimating generalization error.

5.2.2 Limitations of Standard Bootstrapping for Spatial Data

While standard bootstrapping is effective for independent and identically distributed (i.i.d.) data, it faces significant challenges when applied to spatially dependent data:

1. **Violation of Independence Assumption**: Standard bootstrapping assumes observations are independent. In spatial data, nearby observations are correlated, violating this fundamental assumption.

2. **Underestimation of Variance**: Ignoring spatial dependence leads to underestimation of prediction variance, resulting in overly confident inference and narrower-than-appropriate confidence intervals.

3. **Spatial Pattern Disruption**: Random sampling disrupts spatial patterns that are intrinsic to the data's structure, potentially leading to trees that miss important spatial relationships.

4. **Spatial Autocorrelation Transfer**: Trees built on bootstrap samples inherit spatial autocorrelation from the original data, reducing the diversity among trees that random forests rely on.

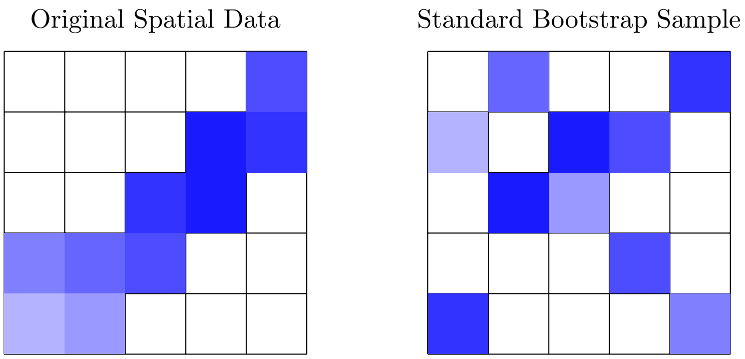

Figure 7: Illustration of how standard bootstrapping disrupts spatial patterns. The original data (left) shows a clear spatial gradient, while the bootstrap sample (right) loses this structure.

5.2.3 Spatial Bootstrapping Alternatives

To address these limitations, several spatial bootstrapping methods have been proposed:

The GLS Bootstrapping Approach Building on the GLS bootstrapping approach introduced in Section 3.2.3, we can formalize a spatial bootstrapping procedure for random forests as follows:

Algorithm 2 GLS Spatial Bootstrap for Random Forests

```
Input: Spatial data $\mathcal{D} = \{(\mathbf{x}_i, y_i, \ell_i)\}_{i=1}^n$, where $\ell_i$ are spatial locations.
Estimate spatial covariance matrix $\hat{\Sigma}$.
Compute Cholesky decomposition $\hat{\Sigma} = \mathbf{L}\mathbf{L}^T$.
Calculate spatially decorrelated residuals:
    $$\mathbf{z} = \mathbf{L}^{-1}(\mathbf{y} - \mathbf{X}\hat{\beta})$$
for $t = 1$ to $T$ do
    Generate bootstrap residuals $\mathbf{z}_t^*$ by resampling from $\mathbf{z}$.
    Create bootstrap response:
        $$\mathbf{y}_t^* = \mathbf{X}\hat{\beta} + \mathbf{L}\mathbf{z}_t^*$$
    Train tree $h_t$ on $\{(\mathbf{x}_i, y_{t,i}^*)\}_{i=1}^n$.
end for
```

This approach ensures that spatial dependence is properly accounted for in the bootstrap samples, leading to more reliable inference.

5.3 Tree Construction in Random Forests

Algorithm 3 GrowTree Procedure

```
procedure GrowTree($h_t, \mathcal{S}, m, n_{\min}$)
    if $|\mathcal{S}| < n_{\min}$ then
        Create leaf node with prediction = average($y$ values in $\mathcal{S}$) for regression
        return
    end if
    Randomly select subset of $m$ features $\mathcal{F} \subset \{1, 2, \ldots, p\}$
    $(j^*, \theta^*) \leftarrow \arg\max_{j \in \mathcal{F}, \theta}$ ImpurityDecrease($\mathcal{S}, j, \theta$)
    if ImpurityDecrease($\mathcal{S}, j^*, \theta^*$) = 0 then
        Create leaf node with prediction based on $\mathcal{S}$
        return
    end if
    Split $\mathcal{S}$ into:
        $\mathcal{S}_L = \{(\mathbf{x}, y) \in \mathcal{S} : x_{j^*} \leq \theta^*\}$
        $\mathcal{S}_R = \{(\mathbf{x}, y) \in \mathcal{S} : x_{j^*} > \theta^*\}$
    Create internal node with split criterion $(j^*, \theta^*)$
    Call GrowTree($h_t, \mathcal{S}_L, m, n_{\min}$) for left child
    Call GrowTree($h_t, \mathcal{S}_R, m, n_{\min}$) for right child
end procedure
```

5.3.1 Classification and Regression Trees (CART) Algorithm

The CART algorithm forms the backbone of individual trees in a random forest. It recursively partitions the feature space to create homogeneous regions with respect to the response variable.

Split Selection Criterion For regression trees, the typical splitting criterion is the reduction in mean squared error (MSE). Given a node τ with data $\mathcal{D}_\tau$, the goal is to find a feature j and threshold s that maximize:

$$\Delta(\tau, j, s) = MSE(\mathcal{D}_\tau) - \frac{|\mathcal{D}_{\tau L}|}{|\mathcal{D}_\tau|} MSE(\mathcal{D}_{\tau L}) - \frac{|\mathcal{D}_{\tau R}|}{|\mathcal{D}_\tau|} MSE(\mathcal{D}_{\tau R}) \tag{4}$$

where $\mathcal{D}_{\tau L} = \{(\mathbf{x}_i, y_i) \in \mathcal{D}_\tau : x_{ij} \leq s\}$ and $\mathcal{D}_{\tau R} = \{(\mathbf{x}_i, y_i) \in \mathcal{D}_\tau : x_{ij} > s\}$ represent the left and right child nodes, respectively.

For classification trees, common splitting criteria include:

Gini Impurity

$$\text{Gini}(\tau) = \sum_{k=1}^{K} \hat{p}_{k\tau}(1 - \hat{p}_{k\tau}) = 1 - \sum_{k=1}^{K} \hat{p}_{k\tau}^2 \tag{5}$$

Entropy

$$\text{Entropy}(\tau) = -\sum_{k=1}^{K} \hat{p}_{k\tau} \log_2(\hat{p}_{k\tau}) \tag{6}$$

where $\hat{p}_{k\tau}$ is the proportion of observations in node τ belonging to class k.

The split is chosen to maximize the reduction in impurity:

$$\Delta(\tau, j, s) = \text{Impurity}(\mathcal{D}_\tau) - \frac{|\mathcal{D}_{\tau L}|}{|\mathcal{D}_\tau|} \text{Impurity}(\mathcal{D}_{\tau L}) - \frac{|\mathcal{D}_{\tau R}|}{|\mathcal{D}_\tau|} \text{Impurity}(\mathcal{D}_{\tau R}) \tag{7}$$

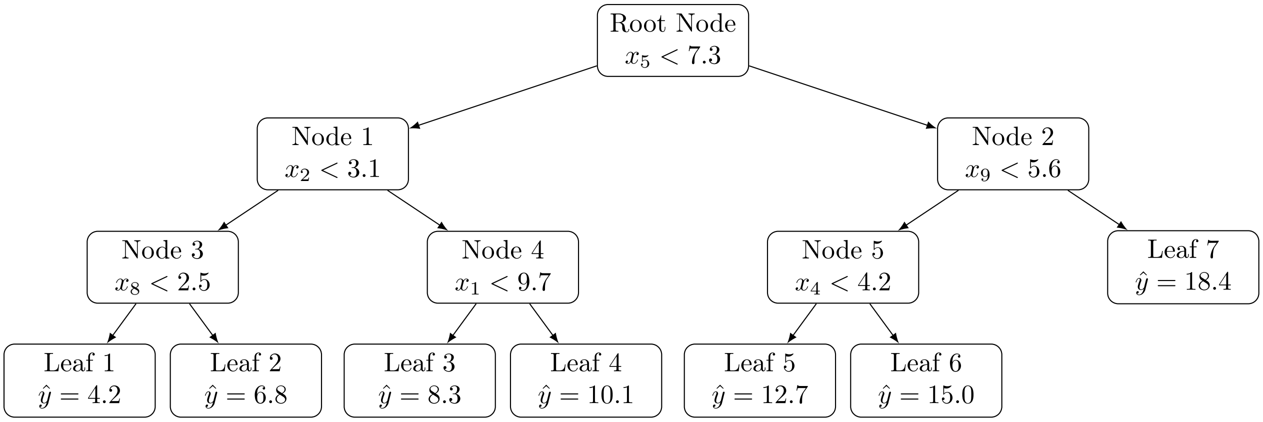

Figure 8: Structure of a decision tree in a random forest. At each non-leaf node, a split is made based on a randomly selected feature subset. Terminal nodes (leaves) contain the prediction values.

5.3.2 Tree Construction Process

5.3.3 Feature Subset Selection

A key aspect of random forests is the random selection of features at each node. For a dataset with p features, only a random subset of m features is considered for each split, where:

- For classification: $m \approx \sqrt{p}$
- For regression: $m \approx p/3$

This feature randomization increases tree diversity and reduces the correlation among trees, improving the performance of the ensemble.

5.4 Random Forest Prediction

5.4.1 Ensemble Prediction Mechanism

The final prediction of a random forest combines the predictions of individual trees:

5.4.2 Out-of-Bag (OOB) Error Estimation

The out-of-bag (OOB) error estimation is a built-in validation mechanism in random forests. Since each tree is trained on approximately 63.2% of the data, the remaining 36.8% (the OOB samples) can be used to estimate generalization error.

For each observation $(\mathbf{x}_i, y_i)$, the OOB prediction is computed using only the trees for which this observation was not in the bootstrap sample:

$$\hat{f}_{OOB}(\mathbf{x}_i) = \frac{1}{|\{t : (\mathbf{x}_i, y_i) \notin \mathcal{D}_t^*\}|} \sum_{t:(\mathbf{x}_i,y_i)\notin\mathcal{D}_t^*} h_t(\mathbf{x}_i) \tag{8}$$

The OOB error estimate is then:

$$\text{OOB Error} = \frac{1}{n}\sum_{i=1}^{n} L(y_i, \hat{f}_{OOB}(\mathbf{x}_i)) \tag{9}$$

where L is a loss function (e.g., mean squared error for regression, misclassification rate for classification).

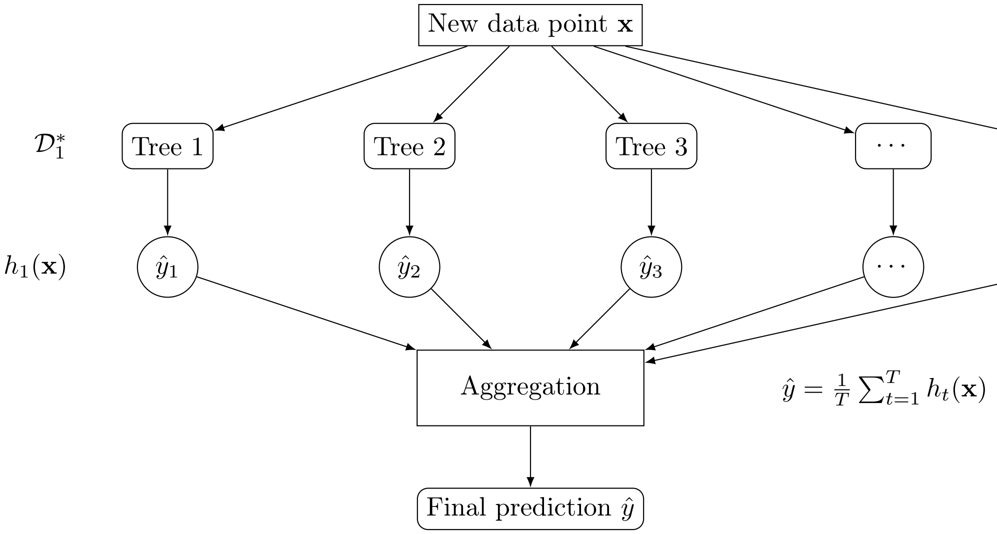

Figure 9: *Random forest prediction process. Each tree produces a prediction based on the input data, and these predictions are then aggregated (averaged for regression, majority vote for classification) to form the final prediction.*

5.5 Variable Importance in Random Forests

5.5.1 Mean Decrease in Impurity (MDI)

The Mean Decrease in Impurity measure quantifies the total reduction in node impurity contributed by a feature across all trees in the forest. For feature j, the importance score is:

$$\text{MDI}(X_j) = \frac{1}{T}\sum_{t=1}^{T}\sum_{\tau \in T_t : v(\tau)=j} p(\tau)\Delta i(\tau) \tag{10}$$

where T_t is the set of nodes in tree t, $v(\tau)$ is the feature used for splitting at node τ, $p(\tau)$ is the proportion of samples reaching node τ, and $\Delta i(\tau)$ is the decrease in impurity at node τ.

5.5.2 Mean Decrease in Accuracy (MDA)

The Mean Decrease in Accuracy, also known as permutation importance, measures the decrease in prediction accuracy when values of a feature are randomly permuted. For feature j, the importance score is:

$$\text{MDA}(X_j) = \frac{1}{T}\sum_{t=1}^{T}(e_{tj} - e_t) \tag{11}$$

where e_t is the OOB error of tree t, and e_{tj} is the OOB error after permuting feature j in the OOB samples for tree t.

6 Covariance Matrix Calculation Methods

6.1 Cholesky Decomposition

Cholesky decomposition is a matrix factorization technique used for positive definite symmetric matrices. Given a symmetric positive definite matrix $\mathbf{A} \in \mathbb{R}^{n\times n}$, the decomposition is:

$$\mathbf{A} = \mathbf{L}\mathbf{L}^T$$

where:

- **L** is a lower triangular matrix with positive diagonal entries.
- $\mathbf{L}^T$ is the transpose of **L**.

This decomposition is particularly useful for solving systems of linear equations, numerical optimization, and statistical computations.

6.1.1 Mathematical Derivation

The elements of **L** can be computed as follows:

Diagonal elements:

$$L_{ii} = \sqrt{A_{ii} - \sum_{k=1}^{i-1} L_{ik}^2}, \quad i = 1, 2, \ldots, n$$

Off-diagonal elements:

$$L_{ij} = \frac{1}{L_{ii}} \left(A_{ij} - \sum_{k=1}^{i-1} L_{ik} L_{jk} \right), \quad j > i$$

6.1.2 Cholesky Decomposition in Spatially Dependent Data

In the context of spatially dependent data, Cholesky decomposition is often used to efficiently compute the inverse of the spatial covariance matrix. Given a covariance matrix $\mathbf{\Sigma}$ derived from a Gaussian Process:

$$\mathbf{\Sigma} = \mathbf{C} + \tau^2 \mathbf{I}$$

where $\mathbf{C}$ is the spatial covariance matrix and $\tau^2 \mathbf{I}$ represents the noise variance, we can factorize it as:

$$\mathbf{\Sigma} = \mathbf{L}\mathbf{L}^T$$

Key Applications This decomposition is crucial for:

- **Efficient inversion** of $\mathbf{\Sigma}$ during Gaussian process regression.
- **Generating samples** from a multivariate normal distribution.
- **Computing the determinant** efficiently, since:

$$\det(\mathbf{\Sigma}) = \prod_{i=1}^{n} L_{ii}^2$$

Implementation Considerations In practical applications, Cholesky decomposition is preferred over direct matrix inversion due to numerical stability and efficiency. When dealing with large-scale spatial data, sparse Cholesky factorizations can further enhance computational efficiency.

6.1.3 Disadvantages of Cholesky Decomposition

Cholesky decomposition is widely used for solving linear systems and Gaussian processes, but it has several drawbacks:

- **Computational Complexity:** It requires $O(n^3)$ operations, making it infeasible for large-scale problems.
- **Memory Requirements:** The full covariance matrix must be stored, leading to $O(n^2)$ memory usage.

- **Numerical Stability:** Small perturbations in the matrix can cause significant errors if it is ill-conditioned.
- **Non-Sparse Structure:** Cholesky decomposition does not inherently exploit sparsity in the covariance matrix.

6.2 Nearest Neighbor Gaussian Process (NNGP)

To overcome these issues, Nearest Neighbor Gaussian Process (NNGP) approximates the full Gaussian process by considering only local dependencies.

Mathematical Formulation: NNGP models the latent function $f(x)$ at a location x_i using its k nearest neighbors:

$$f(x_i)|f(\mathcal{N}(x_i)) \sim \mathcal{N}(\mu_i, K_i) \tag{12}$$

where $\mathcal{N}(x_i)$ represents the set of nearest neighbors, and K_i is the conditional covariance matrix.

Key Advantages:

- Reduces computational cost from $O(n^3)$ to $O(nk^2)$.
- Requires only $O(nk)$ memory instead of $O(n^2)$.
- Preserves local spatial structure efficiently.

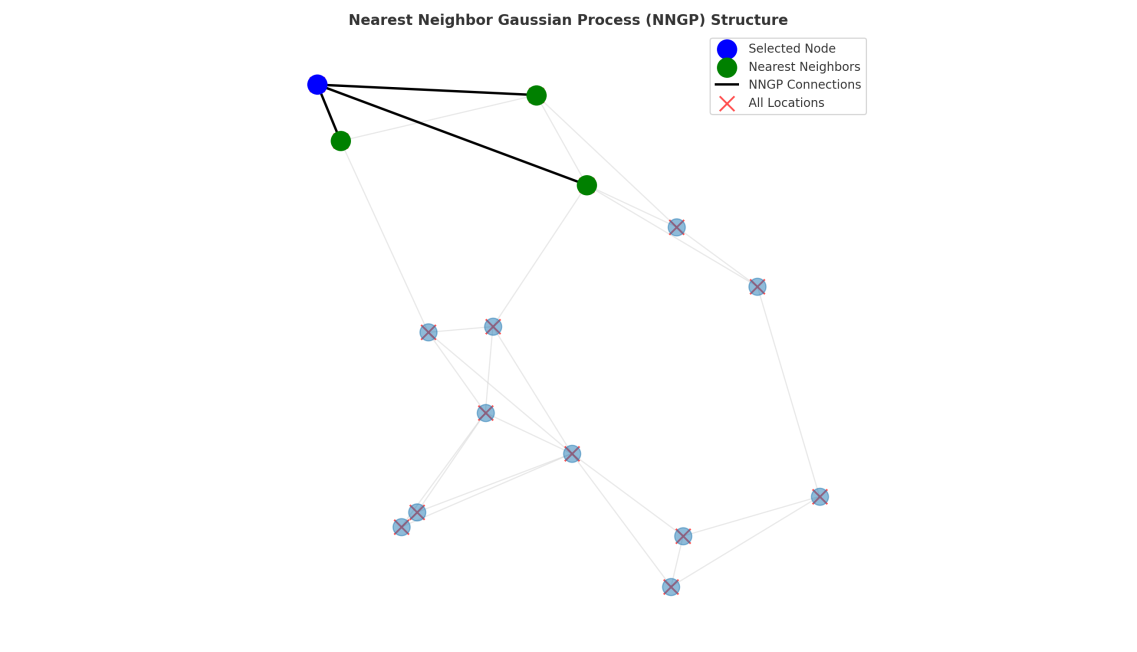

The blue node represents the selected location, green nodes are its nearest neighbors, and black edges show direct dependencies.

Figure 10: *Illustration of NNGP structure*

7 Random Effects Model (REM)

7.1 Theoretical Framework of Random Effects Models

Random effects models are statistical models that account for hierarchical or clustered data structures by incorporating both fixed effects (population-level effects) and random effects (group-specific or cluster-specific variations). These models are particularly valuable when observations are grouped within clusters, such as spatial regions, time periods, or experimental units.

The fundamental concept behind random effects models is the partitioning of variance into components attributable to different levels of the data hierarchy. This allows for proper accounting of correlations among observations within the same group or cluster while maintaining computational efficiency.

7.1.1 Key Characteristics of Random Effects Models

- **Hierarchical Structure**: Random effects models explicitly model the multi-level structure of data, where observations are nested within groups or clusters.
- **Variance Components**: These models decompose the total variance into between-cluster and within-cluster components, allowing for estimation of how much variation exists at each level.
- **Partial Pooling**: Random effects models strike a balance between complete pooling (ignoring group structure) and no pooling (separate models for each group), by "borrowing strength" across groups.
- **Correlation Structure**: Observations within the same cluster are correlated, while observations in different clusters are assumed to be independent.

7.1.2 The Coral Reef Setting as REM

This example clearly demonstrates the hierarchical nature of the data and the importance of accounting for clustering effects.

Problem Setting Consider a study examining the factors affecting coral bleaching intensity across multiple reef regions in the Indo-Pacific:

- Coral reefs (level 1) are nested within geographic regions (level 2)
- Each reef has a bleaching intensity score (Y_{ij}) and reef-level covariates like Maximum Degree Heating Weeks (X_{1ij}) and Community composition (X_{2ij})
- We expect reefs within the same region to have correlated bleaching outcomes due to shared oceanographic conditions, regional climate patterns, and other region-level factors

Mathematical Formulation For reef j in region i, the bleaching intensity can be modeled as:

$$Y_{ij} = \beta_0 + \beta_1 X_{1ij} + \beta_2 X_{2ij} + u_i + \epsilon_{ij} \tag{13}$$

where:

- Y_{ij} is the bleaching intensity for reef j in region i
- X_{1ij} & X_{2ij} are factors like Maximum DHW over 90 days for reef j in region i
- $\beta_0, \beta_1, \beta_2$ are fixed effects (global parameters)
- $u_i \sim N(0, \tau^2)$ is the random effect for region i
- $\epsilon_{ij} \sim N(0, \sigma^2)$ is the residual error for reef j in region i

The random effect u_i represents the deviation of region i from the overall average, after accounting for the measured reef characteristics. It captures the effect of unmeasured region-level factors such as regional oceanographic patterns, historical disturbance regimes, and management practices.

Hierarchical Structure The hierarchical nature of this is visualized in Figure 11.

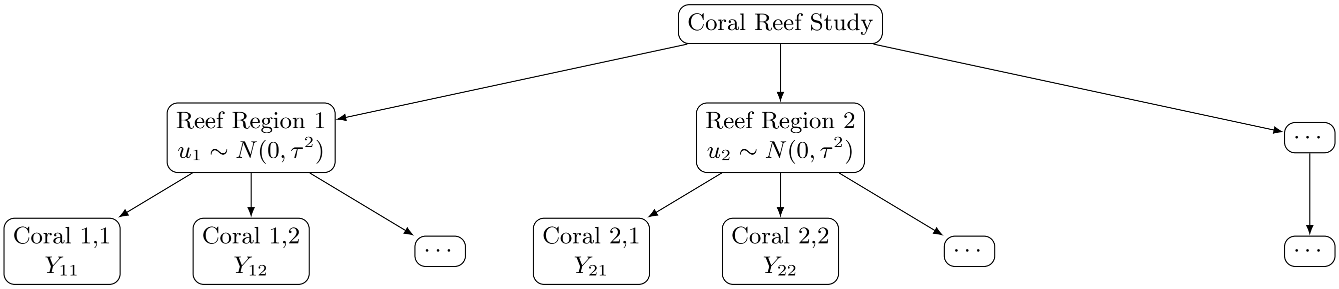

Figure 11: Hierarchical structure demonstration.

Variance Decomposition The total variance in coral bleaching intensity can be decomposed into between-region and within-region components:

$$\begin{aligned}
\mathrm{Var}(Y_{ij}) &= \mathrm{Var}(\beta_0 + \beta_1 X_{1ij} + \beta_2 X_{2ij} + u_i + \epsilon_{ij}) && (14)\\
&= \mathrm{Var}(u_i) + \mathrm{Var}(\epsilon_{ij}) && (15)\\
&= \tau^2 + \sigma^2 && (16)
\end{aligned}$$

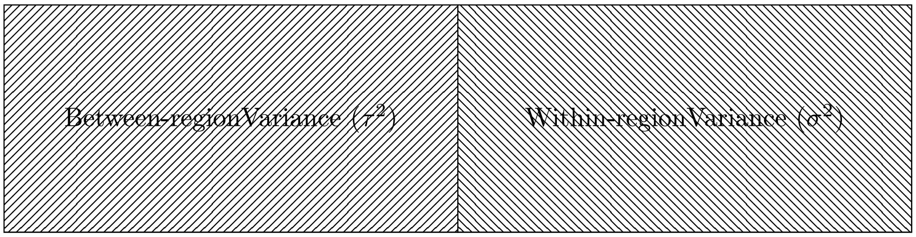
Between-regionVariance (τ^2)
Within-regionVariance (σ^2)

Intraclass Correlation Coefficient (ICC) The ICC measures the proportion of total variance in response attributable to cluster differences:

$$ICC = \frac{\tau^2}{\tau^2 + \sigma^2} \tag{17}$$

BLUP (Best Linear Unbiased Predictor) A key advantage of random effects models is the ability to produce BLUPs for each cluster effect. These estimates are "shrunk" toward the overall mean, with the degree of shrinkage dependent on:

- The number of reefs in the cluster
- The within-cluster variability (σ^2)
- The between-cluster variability (τ^2)

For reef i with n_i coral and mean intensity $\bar{Y}_i$, the BLUP is given by:

$$\hat{u}_i = \frac{\tau^2}{\tau^2 + \sigma^2/n_i} \cdot (\bar{Y}_i - X_i\hat{\beta}) \tag{18}$$

In the context of spatial modeling, random effects models provide a computationally efficient alternative to Gaussian Processes while maintaining the ability to capture spatial correlation structures through cluster-specific effects.

7.2 Model Formulation

Instead of assuming a continuous spatial correlation function as in a GP, we define clusters of locations and introduce random effects at the cluster level. The hierarchical model is given by:

$$Y_{ij} = X_{ij}^T \beta + u_i + \epsilon_{ij} \tag{19}$$

where:

- Y_{ij} is the response for the j-th observation in cluster i.
- X_{ij} is the corresponding feature vector.
- β is the vector of fixed effects.
- $u_i \sim N(0, \tau^2)$ represents the random effect for cluster i.
- $\epsilon_{ij} \sim N(0, \sigma^2)$ is the individual noise.

7.3 Covariance Structure Derivation

7.3.1 Variance of Y_{ij}

Since $X_{ij}^T \beta$ is deterministic, we get:

$$\mathrm{Var}(Y_{ij}) = \tau^2 + \sigma^2 \tag{20}$$

7.3.2 Covariance Within the Same Cluster

For $j \neq j'$:

$$\begin{aligned}
\mathrm{Cov}(Y_{ij}, Y_{ij'}) &= \mathrm{Cov}(u_i + \epsilon_{ij}, u_i + \epsilon_{ij'}) && (21)\\
&= \mathrm{Var}(u_i) + \mathrm{Cov}(u_i, \epsilon_{ij'}) + \mathrm{Cov}(\epsilon_{ij}, u_i) + \mathrm{Cov}(\epsilon_{ij}, \epsilon_{ij'}) && (22)\\
&= \tau^2 && (23)
\end{aligned}$$

7.3.3 Covariance Between Different Clusters

For $i \neq k$:

$$\begin{aligned}
\mathrm{Cov}(Y_{ij}, Y_{kj'}) &= \mathrm{Cov}(X_{ij}^T \beta + u_i + \epsilon_{ij}, X_{kj'}^T \beta + u_k + \epsilon_{kj'}) && (24)\\
&= \mathrm{Cov}(u_i, u_k) + \mathrm{Cov}(\epsilon_{ij}, \epsilon_{kj'}) = 0 && (25)
\end{aligned}$$

7.4 Covariance Matrix Representation

The overall covariance matrix of the Random Effects Model (REM) is derived as follows.

We start with the hierarchical model:

$$Y_{ij} = X_{ij}^T \beta + u_i + \epsilon_{ij} \tag{26}$$

where:

- $u_i \sim N(0, \tau^2)$ is the cluster-level random effect.
- $\epsilon_{ij} \sim N(0, \sigma^2)$ is the individual noise.

Define the full response vector:

$$Y = X\beta + Zu + \epsilon \tag{27}$$

where:

- Z is a block structure matrix mapping observations to clusters.
- $u \sim N(0, \tau^2 I_m)$ represents cluster random effects.
- $\epsilon \sim N(0, \sigma^2 I_n)$ represents independent noise.

The covariance of Y is:

$$\begin{aligned}
\Sigma_{\text{REM}} &= \text{Var}(Y) && (28)\\
&= \text{Var}(X\beta + Zu + \epsilon) && (29)\\
&= Z\text{Var}(u)Z^T + \text{Var}(\epsilon) && (30)\\
&= Z(\tau^2 I_m)Z^T + \sigma^2 I_n && (31)
\end{aligned}$$

Since ZZ^T creates a block structure, we obtain:

$$\Sigma_{\text{REM}} = \tau^2 J_m + \sigma^2 I_n \tag{32}$$

where:

- J_m is a block matrix capturing intra-cluster correlation.
- I_n is an identity matrix capturing independent noise.

7.5 Computational Complexity of Random Effects Model (REM)

The computational complexity of the Random Effects Model (REM) primarily arises from inverting the covariance matrix, given by:

$$\Sigma_{\text{REM}} = \tau^2 J_m + \sigma^2 I_n, \tag{33}$$

where:

- J_m is a block matrix capturing intra-cluster correlations,
- I_n is the identity matrix representing independent noise,
- τ^2 and σ^2 are variance parameters.

7.5.1 Complete Structure of the Covariance Matrix

Let's examine J_m more precisely. For a dataset with m clusters, each containing k observations (so $n = mk$ total observations), J_m is a block diagonal matrix:

$$J_m = \begin{bmatrix} \mathbf{1}_{k\times k} & \mathbf{0} & \cdots & \mathbf{0} \\ \mathbf{0} & \mathbf{1}_{k\times k} & \cdots & \mathbf{0} \\ \vdots & \vdots & \ddots & \vdots \\ \mathbf{0} & \mathbf{0} & \cdots & \mathbf{1}_{k\times k} \end{bmatrix} \tag{34}$$

where $\mathbf{1}_{k\times k}$ is a $k \times k$ matrix of all ones, representing perfect correlation within each cluster.

7.5.2 Kronecker Product Representation

Using the Kronecker product notation:

$$J_m = I_m \otimes \mathbf{1}_{k\times k} \tag{35}$$

This means J_m is constructed by replacing each 1 in the $m \times m$ identity matrix with a $k \times k$ matrix of all ones.

7.5.3 Applying the Woodbury Matrix Identity

To efficiently compute Σ_{REM}^{-1}, we apply the Woodbury matrix identity:

$$(A + UCV)^{-1} = A^{-1} - A^{-1}U(C^{-1} + VA^{-1}U)^{-1}VA^{-1} \tag{36}$$

For our case, we set:

- $A = \sigma^2 I_n$
- $U = \sqrt{\tau^2} \cdot Z$, where Z is the design matrix mapping observations to clusters
- $C = I_m$
- $V = \sqrt{\tau^2} \cdot Z^T$

The design matrix Z is an $n \times m$ matrix where $Z_{ij} = 1$ if observation i belongs to cluster j, and 0 otherwise.

This gives us:

$$\Sigma_{\text{REM}} = \sigma^2 I_n + \tau^2 ZZ^T \tag{37}$$

Now we can apply the Woodbury identity:

$$\Sigma_{\text{REM}}^{-1} = \frac{1}{\sigma^2} I_n - \frac{1}{\sigma^4} Z(I_m + \frac{\tau^2}{\sigma^2} Z^T Z)^{-1} Z^T \tag{38}$$

7.5.4 Computational Breakdown

- Computing $Z^T Z$ requires $O(nm)$ operations, resulting in an $m \times m$ matrix.
- Computing $(I_m + \frac{\tau^2}{\sigma^2} Z^T Z)$ requires $O(m^2)$ operations.
- Inverting the $m \times m$ matrix $(I_m + \frac{\tau^2}{\sigma^2} Z^T Z)^{-1}$ requires $O(m^3)$ operations.
- Multiplying Z by this inverted matrix and then by Z^T requires $O(nm) + O(nm) = O(nm)$ operations.
- The final subtraction to get Σ_{REM}^{-1} requires $O(n)$ operations.

7.5.5 Exploiting Structure for Additional Efficiency

We can further exploit the block structure of J_m. Since each cluster has identical structure:

$$Z^T Z = \text{diag}(k, k, \ldots, k) = k \cdot I_m \tag{39}$$

This simplifies to:

$$\Sigma_{\text{REM}}^{-1} = \frac{1}{\sigma^2} I_n - \frac{\tau^2}{\sigma^2(\sigma^2 + k\tau^2)} ZZ^T \tag{40}$$

The computational complexity is further reduced because $(I_m + \frac{\tau^2}{\sigma^2} Z^T Z)^{-1} = (I_m + \frac{k\tau^2}{\sigma^2} I_m)^{-1} = \frac{\sigma^2}{\sigma^2 + k\tau^2} I_m$, which is a scalar multiplication that requires only $O(1)$ operations.

7.5.6 Final Complexity Conclusion

The dominant term in the computational complexity is the $O(m^3)$ operation for inverting the $m \times m$ matrix. Since $m \ll n$ (the number of clusters is much smaller than the total number of observations), REM achieves significantly lower complexity than Gaussian Processes, where inverting an $n \times n$ covariance matrix requires $O(n^3)$ operations.

In many practical scenarios with large datasets but a moderate number of clusters, this reduction from $O(n^3)$ to $O(m^3)$ makes REM computationally tractable while still capturing important correlation structures.

7.6 Comparison with Gaussian Process (GP)

Table 2: Comparison of Random Effects Model (REM) and Gaussian Process (GP)

Aspect	Random Effects Model (REM)	Gaussian Process (GP)
Covariance Structure	$\Sigma_{\text{REM}} = \tau^2 J_m + \sigma^2 I_n$	$\Sigma_{\text{GP}} = C(S, S) + \sigma^2 I_n$
Interpretation	Constant correlation within clusters	Kernel-based spatial correlations
Computational Complexity	$O(m^3)$ (where $m \ll n$)	$O(n^3)$ due to matrix inversion
Scalability	Suitable for large datasets	Computationally expensive
Assumptions	Independent clusters	Smooth spatial correlation

8 Final Proposed Model

The **RandomForestREM** algorithm integrates spatial clustering, residual error modeling, and random forest regression to effectively address spatial dependencies in data. It begins by applying K-means clustering on spatial coordinates to group observations into spatial clusters. Using **Likelihood Estimation**, it estimates spatial covariance parameters (σ^2 and τ^2) for each cluster, accounting for spatial autocorrelation. A covariance matrix is then constructed based on these estimates, which is incorporated into a **Generalized Least Squares (GLS)** framework to generate spatially-aware bootstrap samples. Random forests are trained on these bootstrap samples for each cluster, ensuring that spatial dependencies are preserved during model training. The final model aggregates predictions from all clusters, resulting in improved accuracy and robust handling of spatially correlated data.

8.1 Random Effect Model Specification & Covariance Matrix Estimation

We consider a linear mixed effects model with a random intercept. Let y_{ij} denote the response for the i-th observation in the j-th cluster. The model is given by:

$$y_{ij} = X_{ij}\beta + u_j + \epsilon_{ij}$$

where:

- X_{ij} is the row vector of covariates for observation (i, j),
- $\beta \in \mathbb{R}^p$ is the vector of fixed effects,
- $u_j \sim \mathcal{N}(0, \tau^2)$ is the random intercept for cluster j,
- $\epsilon_{ij} \sim \mathcal{N}(0, \sigma^2)$ is the independent noise.

We assume that u_j and ϵ_{ij} are independent.

Let $y_j \in \mathbb{R}^{n_j}$ denote the vector of responses in cluster j, and let $X_j \in \mathbb{R}^{n_j \times p}$ be the corresponding matrix of covariates. Define $Z_j = \mathbf{1}_{n_j}$ (a vector of ones), then the model can be written compactly as:

$$y_j = X_j\beta + Z_j u_j + \epsilon_j$$

8.2 Marginal Distribution of Responses

By integrating out the random effect u_j, we obtain the marginal distribution:

$$y_j \sim \mathcal{N}(X_j\beta, V_j)$$

where the marginal covariance matrix V_j is given by:

$$V_j = \tau^2 Z_j Z_j^\top + \sigma^2 I_{n_j} = \tau^2 J_{n_j} + \sigma^2 I_{n_j}$$

Here, J_{n_j} is an $n_j \times n_j$ matrix of ones.

8.3 Log-Likelihood Function

The log-likelihood function (ignoring additive constants) over all clusters $j = 1, \dots, J$ is:

$$\ell(\beta, \sigma^2, \tau^2) = -\frac{1}{2}\sum_{j=1}^{J}\left(\log|V_j| + (y_j - X_j\beta)^\top V_j^{-1}(y_j - X_j\beta)\right)$$

8.4 Maximum Likelihood Estimation Procedure

We estimate the parameters $(\beta, \sigma^2, \tau^2)$ by maximizing the log-likelihood function. The procedure is as follows:

1. **Initialization:** Start with initial guesses for τ^2 and σ^2, for example, 1.0.
2. **Estimate β given τ^2 and σ^2:** Use Generalized Least Squares (GLS):

$$\hat{\beta} = \left(\sum_{j=1}^{J} X_j^\top V_j^{-1} X_j\right)^{-1}\left(\sum_{j=1}^{J} X_j^\top V_j^{-1} y_j\right)$$

3. **Compute Residuals:** For each cluster,

$$r_j = y_j - X_j\hat{\beta}$$

4. **Update τ^2 and σ^2:** Maximize the log-likelihood (or minimize the negative log-likelihood) with respect to τ^2 and σ^2:

$$\ell(\tau^2, \sigma^2) = -\frac{1}{2}\sum_{j=1}^{J}\left(\log|V_j| + r_j^\top V_j^{-1} r_j\right)$$

   This can be done numerically using optimization methods such as Newton-Raphson or quasi-Newton techniques.

5. **Iterate:** Repeat steps 2–4 until convergence.

8.5 MLE Estimates

Once the optimization converges, we obtain the maximum likelihood estimates:

- $\hat{\beta}$: fixed effect
- $\hat{\sigma}^2$: residual variance
- $\hat{\tau}^2$: random effect variance

These estimates can be used for subsequent inference or bootstrapping within the random effects framework.

8.6 Why the proposed algorithm RF-REM Works?

- **Addressing Spatial Autocorrelation:** Spatial autocorrelation refers to the tendency of nearby spatial units to exhibit similar values. Traditional models often ignore this dependency, leading to biased estimates. In contrast, spatial mixed models or geostatistical approaches use a covariance matrix (V) that explicitly accounts for these dependencies:
  - τ^2 represents the *between-cluster variance*, capturing correlations between different spatial clusters or regions.
  - σ^2 denotes the *within-cluster variance*, accounting for local noise and variability inside a spatial unit.

  This structure enables the model to differentiate between global spatial trends and local fluctuations.

- **Statistical Benefits of Covariance Modeling:**
  - *Whitening Transformation:* By leveraging the covariance structure, the model transforms spatially correlated data into an approximately independent space, simplifying inference and reducing bias.
  - *Reliable Uncertainty Estimates:* Accounting for spatial correlation avoids underestimation of uncertainty, leading to more accurate confidence intervals and standard errors.
  - *Valid Inference:* Classical statistical tests often assume independence. Incorporating spatial dependence restores the validity of these tests, allowing for sound hypothesis testing and interpretation.

- **Improved Prediction through Clustering:**
  - *Locally Varying Relationships:* Instead of assuming a single global model, clustering allows the model to capture different predictor-response relationships across spatial regions.
  - *Context-Aware Prediction:* New observations can be assigned to clusters with similar spatial characteristics, ensuring more contextually accurate predictions.
  - *Adaptability:* The model can adapt to heterogeneous spatial processes, such as varying terrain, climate, or land use patterns.

- **Practical Advantages:**
  - *Accurate Variable Importance:* Spatial permutation methods provide more robust measures of feature importance by considering spatial structure during randomization.
  - *Reduced Overfitting:* By modeling spatial structure explicitly, the model avoids capturing noise as meaningful spatial patterns, reducing overfitting.
  - *Superior Real-World Performance:* These models are particularly effective in applications like environmental monitoring, geographical modeling, and epidemiology, where spatial structure is intrinsic to the data.
  - *Enhanced Interpretability of Spatial Effects:* Modeling spatial components provides interpretable insights into the underlying structure of spatial variation. For instance, in spatial mixed models:
    - The total variance can be decomposed into spatial and non-spatial components: $\frac{\tau^2}{\tau^2+\sigma^2}$ quantifies the proportion of variation due to spatial effects.
    - This helps identify whether spatial location is a major driver of the response variable.
    - It enables visualization of spatial random effects, revealing latent spatial risk or spatial disparities that may not be explained by observed covariates.
    - In policy or public health, this informs geographically targeted interventions where spatial effects are dominant.

The covariance structure fundamentally transforms how the algorithm learns from spatial data by properly accounting for the non-independence of observations across space, leading to models that better capture true underlying relationships rather than spatial noise. The pseudo code for the complete algorithm is provided below.

Algorithm 4 RandomForestREM Algorithm

```
procedure RandomForestREM($X, y, coords, n\_estimators, n\_clusters, n\_bootstraps$)
    Initialize parameters ($n\_estimators, max\_features, min\_samples\_leaf, etc.$)
end procedure
procedure InitializeClusters($X, coords$)
    Apply K-means to $coords$ with $k = n\_clusters$ & assign cluster labels to observations
    return cluster labels
end procedure
procedure EstimateCovarianceParametersREML($X, y$)
    Train vanilla RF to obtain residuals $r = y - \hat{y}$
    Define cluster indicator matrix $Z$ where $Z_{ij} = 1$ if observation $i$ in cluster $j$
    Define REML negative log-likelihood function:
    function REML_NegLogLik($\tau^2, \sigma^2$)
        Construct covariance matrix $V$ where:
        $V_{ii} = \sigma^2 + \tau^2$ for diagonal elements
        $V_{ij} = \tau^2$ if observations $i, j$ in same cluster, 0 otherwise
        return negative log-likelihood
    end function
    Estimate $\tau^2, \sigma^2$ by minimizing REML_NegLogLik
    return $\sigma^2, \tau^2$
end procedure
procedure ConstructREMCovariance($n\_samples$)
    Set diagonal elements: $Cov_{ii} = \tau^2 + \sigma^2$
    For each cluster $k$:
      Set $Cov_{ij} = \tau^2$ for all pairs $(i, j)$ in cluster $k$ where $i \neq j$
    return $Cov$
end procedure
procedure GLSBootstrap($X, y, n\_samples$)
    Construct covariance matrix $Cov$ using ConstructREMCovariance
    Compute whitened data: $X_w = L^{-1}X$, $y_w = L^{-1}y$
    Train RF model on whitened data, get fitted values $\hat{y}_w$
    Compute whitened residuals $r_w = y_w - \hat{y}_w$
    for $b = 1$ to $n\_samples$ do
        Sample with replacement from $r_w$ to get $r_w^*$
        Generate bootstrap response: $y_w^* = \hat{y}_w + r_w^*$
        Transform back: $y^* = Ly_w^*$ & Store bootstrap sample $(X, y^*)$
    end for
    return bootstrap samples
end procedure
procedure TrainBootstrapTree($X\_boot, y\_boot, tree\_idx$)
    Initialize single tree RF with appropriate parameters & Train tree on bootstrap sample
    return trained tree
end procedure
procedure Fit($X, y, coords$)
    Initialize spatial clusters from $coords$ & Estimate covariance parameters $\sigma^2, \tau^2$ via REML
    $cluster\_models \leftarrow \emptyset$
    for each unique cluster $c$ do
        Extract observations: $X_c \leftarrow X[cluster\_labels = c]$, $y_c \leftarrow y[cluster\_labels = c]$
        Train RF model on $(X_c, y_c)$, Store model, $\mathrm{R}^2$ score, and size for cluster $c$
    end for
    Compute $\mathrm{R}^2$ score
    return fitted model
end procedure
```

8.7 Results

- The proposed Random Forest with Random Effects Model (RF-REM) achieved an R^2 value of **0.8842**, outperforming all prior models.
- **Comparison with previous models:**
  - Simple Linear Regression: $R^2 = 0.5212$
  - Spatial Linear Regression: $R^2 = 0.6740$
  - Generalized Additive Model (GAM): $R^2 = 0.8423$
  - Clustering-based Random Forest: Weighted $R^2 = 0.5804$
- **Reasons for improved performance:**
  - Explicitly models spatial autocorrelation via cluster-level random effects.
  - Captures both inter-cluster and intra-cluster variability, which previous models missed.
  - Uses spatial bootstrapping to preserve correlation structures during resampling.
  - Leverages the non-linear modeling strength of Random Forest with statistical rigor of Random Effects Models.
  - Provides more reliable inference and reduces prediction bias due to spatial dependence.
- **Practical impact:**
  - Offers improved interpretability of spatial patterns in coral bleaching.
  - Demonstrates that integrating machine learning with hierarchical modeling is effective for spatial environmental data.
- **Feature importance and analysis**
  - Feature importance was assessed using methods like Mean Decrease in Impurity (**MDI**) and a cluster-aware **permutation** approach that estimates importance by evaluating the performance drop when features are randomly shuffled within spatial clusters.

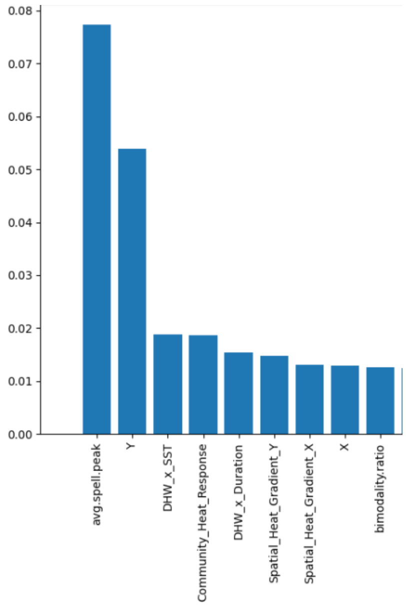

Figure 12: Top features based on model-agnostic importance.

- avg_spell_peak was the most influential feature, highlighting the role of acute thermal extremes in coral bleaching.
- Spatial coordinates (Y, X) showed strong importance, consistent with spatial heterogeneity in heat exposure.
- Interaction terms (DHW_x_SST, DHW_x_Duration) were key, capturing nonlinear thermal stress effects.
- Community_Heat_Response and bimodalityratio reflect biological resilience and environmental variability.
- Variables like habitat and management had minimal influence in both linear and nonlinear settings.

9 Conclusion

This project successfully integrated Random Forest methodology with Random Effects Models to address spatial autocorrelation in environmental data, specifically for coral bleaching prediction across the Indo-Pacific. Our Spatial Random Forest with REM approach achieved superior performance ($R^2 = 0.88$) compared to traditional methods, including a previous study by **McClanahan et al.** 2019, which reported a maximum $R^2 = 0.52$ using conventional approaches. This highlights the effectiveness of our methodology in capturing the complex spatial patterns governing coral bleaching. Moreover, our method maintains reasonable computational complexity ($O(m^3)$). Key methodological contributions include a spatial bootstrapping framework that preserves correlation structures and a hierarchical modeling approach capturing both between-cluster and within-cluster spatial variability. Feature importance was assessed using methods like Mean Decrease in Impurity (MDI) and a cluster-aware permutation approach that estimates importance by evaluating the performance drop when features are randomly shuffled within spatial clusters. This analysis revealed that avg_spell_peak was the most influential predictor, emphasizing the critical role of acute thermal extremes in coral bleaching. Spatial coordinates (Y, X) also showed strong importance, reflecting spatial heterogeneity in heat exposure across reef systems. Interaction terms such as DHW_x_SST and DHW_x_Duration were also key, capturing nonlinear effects of thermal stress. Variables like Community_Heat_Response and bimodalityratio reflected biological resilience and environmental variability, while features such as habitat type and management zone had minimal influence in both linear and nonlinear settings. Despite limitations in cluster definition, temporal dynamics, and distributional assumptions, our framework demonstrates that combining machine learning with mixed-effects models effectively analyzes spatially dependent environmental data. By addressing spatial autocorrelation challenges, this approach enables more accurate predictions of ecological responses to environmental change, supporting evidence-based conservation strategies for vulnerable coral reef ecosystems. Future work should explore adaptive clustering methods, spatio-temporal extensions, non-Gaussian variants, and Bayesian implementations to further enhance this promising framework.

References

Tracy D Ainsworth, Scott F Heron, Juan Carlos Ortiz, Peter J Mumby, Alana Grech, Daisie Ogawa, C Mark Eakin, and William Leggat. Climate change disables coral bleaching protection on the great barrier reef. *Science*, 352(6283):338–342, 2016.

Sudipto Banerjee, Bradley P Carlin, and Alan E Gelfand. *Hierarchical modeling and analysis for spatial data*. CRC press, 2014.

D Richard Cutler, Thomas C Edwards Jr, Karen H Beard, Adele Cutler, Kyle T Hess, Jonathan Gibson, and Joshua J Lawler. Random forests for classification in ecology. *Ecology*, 88(11):2783–2792, 2007.

Tomislav Hengl, Madlene Nussbaum, Marvin N Wright, Gerard BM Heuvelink, and Benedikt Gräler. Random forest as a generic framework for predictive modeling of spatial and spatio-temporal variables. *PeerJ*, 6:e5518, 2018.

Ove Hoegh-Guldberg, Elvira S Poloczanska, William Skirving, and Sophie Dove. Coral reef ecosystems under climate change and ocean acidification. *Frontiers in Marine Science*, 4:158, 2017.

Terry P Hughes, James T Kerry, Andrew H Baird, Sean R Connolly, Andreas Dietzel, C Mark Eakin, Scott F Heron, Andrew S Hoey, Mia O Hoogenboom, Gang Liu, et al. Global warming transforms coral reef assemblages. *Nature*, 556(7702):492–496, 2018.

Jin Li, Andrew D Heap, Anna Potter, and James J Daniell. Application of machine learning methods to spatial interpolation of environmental variables. *Environmental Modelling & Software*, 26(12):1647–1659, 2011.

Tim R McClanahan, Emily S Darling, Joseph M Maina, Nyawira A Muthiga, Stéphanie D'agata, Stacy D Jupiter, Rohan Arthur, Shaun K Wilson, Sangeeta Mangubhai, Yashika Nand, et al. Temperature patterns and mechanisms influencing coral bleaching during the 2016 el niño. *Nature Climate Change*, 9(11):845–851, 2019. doi: 10.1038/s41558-019-0576-8. URL `https://doi.org/10.1038/s41558-019-0576-8`.

Hanna Meyer, Christoph Reudenbach, Stephan Wöllauer, and Thomas Nauss. Importance of spatial predictor variable selection in machine learning applications–moving from data reproduction to spatial prediction. *Ecological Modelling*, 411:108815, 2019.

David R Roberts, Volker Bahn, Simone Ciuti, Mark S Boyce, Jane Elith, Gurutzeta Guillera-Arroita, Severin Hauenstein, José J Lahoz-Monfort, Boris Schröder, Wilfried Thuiller, et al. Cross-validation strategies for data with temporal, spatial, hierarchical, or phylogenetic structure. *Ecography*, 40(8):913–929, 2017.

Arkajyoti Saha, Sumanta Basu, and Abhirup Datta. Random forests for spatially dependent data. *Journal of the American Statistical Association*, 118(541):665–683, 2023. doi: 10.1080/01621459.2021.1950003. URL `https://doi.org/10.1080/01621459.2021.1950003`.

Roozbeh Valavi, Jane Elith, José J Lahoz-Monfort, and Gurutzeta Guillera-Arroita. blockcv: An r package for generating spatially or environmentally separated folds for k-fold cross-validation of species distribution models. *Methods in Ecology and Evolution*, 10(2):225–232, 2019.

Simon N Wood. Generalized additive models: an introduction with r. *CRC press*, 2017.